Journal of Anatomy

J. Anat. (2016) doi: 10.1111/joa.12563

Quantum dots labelling allows detection of the homing of mesenchymal stem cells administered as immunomodulatory therapy in an experimental model of pancreatic islets transplantation

Silvia Mannucci,[1] Laura Calderan,[1] Paola Quaranta,[2] Sara Antonini,[2] Franco Mosca,[2] Biancamaria Longoni,[2] Pasquina Marzola[3] and Federico Boschi[3]

[1]*Department of Neuroscience, Biomedicine and Movement, University of Verona, Verona, Italy*
[2]*Department of Translational Research and of New Surgical and Medical Technologies, University of Pisa, Pisa, Italy*
[3]*Department of Computer Science, University of Verona, Verona, Italy*

Abstract

Cell transplantation is considered a promising therapeutic approach in several pathologies but still needs innovative and non-invasive imaging technologies to be validated. The use of mesenchymal stem cells (MSCs) attracts major interest in clinical transplantation thanks to their regenerative properties, low immunogenicity and ability to regulate immune responses. In several animal models, MSCs are used in co-transplantation with pancreatic islets (PIs) for the treatment of type I diabetes, supporting graft survival and prolonging normal glycaemia levels. In this study we investigated the homing of systemically administered MSCs in a rat model of pancreatic portal vein transplantation. MSCs labelled with quantum dots (Qdots) were systemically injected by tail vein and monitored by optical fluorescence imaging. The fluorescence signal of the liver in animals co-transplanted with MSCs and PIs was significantly higher than in control animals in which MSCs alone were transplanted. By using magnetic labelling of PIs, the homing of PIs into liver was independently confirmed. These results demonstrate that MSCs injected in peripheral blood vessels preferentially accumulate into liver when PIs are transplanted in the same organ. Moreover, we prove that bimodal MRI-fluorescence imaging allows specific monitoring of the fate of two types of cells.

Key words: fluorescence imaging; magnetic resonance imaging; mesenchymal stem cells; pancreatic islets; quantum dots; transplantation.

Introduction

Cell transplantation is considered a promising therapeutic approach in several pathologies including neurological (De Feo et al. 2012), cancerous (Aly, 2012), musculoskeletal (Nie et al. 2012), and metabolic diseases (Longoni et al. 2010). Among cell-based therapies, stem cells (SCs) evoke great interest due to their ability to self-renew and to differentiate into multiple cell lineages (Wei et al. 2013). To be used safely in clinical settings, SCs should demonstrate genomic stability, be readily harvested and/or expanded and, above all, not induce teratomas (Sohni & Verfaillie, 2013). Embryonic stem cells (ESCs), which can be derived from blastocyst, are pluripotent cells displaying genomic stability (Evans & Kaufman, 1981; Yoon et al. 2014). Beyond the ethical concerns due to their origin, ESCs can induce teratoma formation *in vivo* (Przyborski, 2005; Blum & Benvenisty, 2008) and may elicit tissue rejection following transplantation in patients. The advent of induced pluripotent stem cell, discovered in 2006 by Takahashi and Gurdon (Gurdon, 2006; Takahashi & Yamanaka, 2006), opened new perspectives for SC therapy. These cells can indeed be obtained by reprogramming differentiated adult cells, overcoming limitations due to ethical concerns, and can be differentiated in any lineages. However, to be considered clinically safe, their genomic stability still needs to be established (Ullah et al. 2015).

Mesenchymal stem cells (MSCs), which are adult stem cells of mesodermal origin, are free from ethical concerns, thus becoming a promising candidate for cell therapies (Horwitz et al. 2005). Along with multi-potency and self-renewal, MSCs lack the co-stimulatory molecules of the class II major

Correspondence
Federico Boschi and Silvia Mannucci, Department of Computer Science, University of Verona, Strada Le Grazie 15, I-37134 Verona, Italy. E: federico.boschi@univr.it (FB), silvia.mannucci@univr.it (SM)

Accepted for publication *11 October 2016*

histocompatibility complex (MHC II); moreover, they exhibit immunosuppressive properties; their overall immunological features and low immunogenicity makes them an attractive tool for the development of transplantation approaches (Patel et al. 2008). The use of MSCs in association with pancreatic islets (PIs) in animal transplants has been largely investigated for the treatment of type I diabetes (Ricordi & Strom, 2004; Domínguez-Bendala et al. 2012), a pathology characterized by the irreversible autoimmune destruction of pancreatic beta cells (Sakata et al. 2010). Islet transplantation in the portal vein of patients affected by type I diabetes combines minimally invasive surgery with low incidence of peri-operative risks (Weimar et al. 1999) while improving glycaemic control and prospective insulin independence (Sutherland et al. 1993; Bretzel et al. 1995; Hogan et al. 2008). We recently reported that co-transplantation of MSCs and PIs helps to prolong normal glycaemic levels in an experimental model of chemically induced diabetes in rats (Longoni et al. 2010). The effect of the intravenous administration of MSCs was assessed in both an allogeneic and a syngeneic model. PIs transplanted in the portal vein engrafted into the liver as demonstrated by *in vivo* imaging studies (Marzola et al. 2009; Arifin & Bulte, 2011). Several papers showed that when MSCs are injected systemically they preferentially distribute to a wide variety of organs, i.e. spleen and lungs (with cell entrapment triggered by MSCs dimensions) (Vittorio et al. 2011), resulting in a loss of therapeutic efficacy. Therefore additional investigations of the stem cell homing are required to improve the efficacy of cell therapies. Non-invasive imaging techniques such as magnetic resonance imaging (MRI), optical imaging (OI) and positron emission tomography (PET) are widely used to visualize cells *in vivo* in intact organisms after labelling cells with magnetic (Sykova & Jendelova, 2007; Oishi et al. 2013), fluorescent (Yukawa et al. 2012) or radioactive (Wu et al. 2013) probes, prior to their transplantation. We reported that PIs can be labelled with superparamagnetic iron oxide particles (SPIOs) and visualized in the liver of the recipient subject by MRI with high sensitivity (Marzola et al. 2009; Arifin & Bulte, 2011). Furthermore, several articles have shown that SCs can also be labelled with superparamagnetic particles without relevant cytotoxic effects and detected with high sensitivity *in vivo* by MRI. In the present study, MSCs and PIs were co-transplanted within the same experimental procedure and visualized with two different imaging techniques. PIs are easily detectable using SPIO labelling and MRI as demonstrated in our previous work (Marzola et al. 2009; Longoni et al. 2010). To image MSCs we decided to use as a fluorescent probe quantum dots (Qdots), which are specifically designed for cell labelling. Qdots emitting in the near infrared range, i.e. inside the transparency window of living tissue, were chosen. The attenuation of light in biological tissues depends on the combined effect of light absorption and scattering, well expressed by the inverse exponential power law (Beer–Lamberts Law). Increasing the depth of the light source, the signal highly decreases, so due to the thickness of rat tissues, we were forced to work *ex vivo* by acquiring fluorescence images of excised organs rather than working *in vivo*. The presence of the PI into the liver was demonstrated by our previous studies (Marzola et al. 2009; Longoni et al. 2010) and confirmed by this study. Our data clearly demonstrate that MSCs, injected immediately after PI transplantation during the same experimental procedure, were driven into the liver to a greater extent compared with control animal, in which MSCs alone were administered. The novelty of our approach provides the proof of concept that bimodal labelling of two different kind of cells and the use of a bimodal imaging modality can be used to unveil cellular homing when the two types of cells are transplanted.

Materials and methods

Animals

Inbred male Lewis (L) (n = 36) and Wistar Furth (WF) (n = 20) rats, weighing 275–300 g, were purchased from Charles River Laboratories (Italy). The animals, fed on standard rodent chow (Rieper, Italy) and water *ad libitum*, were kept in a 12 h light/dark cycle. In our experimental model, WF rats were used as donors and L rats as recipients of PIs. All experimental procedures were carried out with the approval of the Ethical Committee for Animal Experimentation of the University of Pisa.

MSC isolation and culture

MSCs and bone marrow cells were collected from both tibias and femurs of L rats following Dobson's procedure (Dobson et al. 1999). Total nucleated cells were cultured in Dulbecco's modified culture medium (DMEM; Sigma-Aldrich, Italy) supplemented with 10% fetal bovine serum (FBS; Eurobio, Italy), 1% L-glutamine (Sigma-Aldrich), penicillin (50 μg mL^{-1}; Eurobio), streptomycin (50 μg mL^{-1}; Eurobio), amphotericin B (0.2 μg mL^{-1}; Sigma-Aldrich), and incubated at 37 °C in a fully humidified atmosphere containing 95% air and 5% carbon dioxide. After 7 days, half of the culture medium was changed. On reaching confluence, the adherent cells were detached by 0.05% trypsin and 0.02% EDTA for 5–10 min at 37 °C, harvested and washed with Hanks' balanced salt solution (HBSS) and 10% FBS and finally re-suspended in complete medium (primary culture, P0). Cells were re-seeded at 10^4 cells cm^{-2} in 100-mm dishes (P1) for both *in vitro* differentiation assessment and subsequent cellular expansion, which was achieved by successive cycles of trypsinization and re-seeding. The frequency of colony forming units-fibroblasts (CFU-F) was measured using the method of Castro-Malaspina (Gay et al. 1980). Visible colonies with 50 or more cells (the conventional value for defining a colony) were counted and referred to 10^6 plated cells (no. of CFU-F/10^6 TNC).

In vitro experiments

MSCs were labelled with Qdots (Qtracker® 800 kit cell labelling; Invitrogen™ Milan, Italy) following the datasheet instructions. Briefly, 10 nmol Qdots were added to MSCs in T75 flask. After 1 h,

the adherent cells were detached by 0.05% trypsin/EDTA (Life Technology, Italy), counted, centrifuged at 150 g, washed three times in phosphate buffered saline (PBS) and re-suspended in 300 μL of DMEM without FBS. After labelling, the fluorescence signal of MSCs was measured *in vitro*. Different amounts of labelled cells (range 50–10^5 cells) were suspended in non-fluorescent wells and acquired by OI in the fluorescence modality using the same experimental setup as in the excised organs acquisition protocol (Fig. 1C).

Pancreatic islets isolation, culture and labelling

Pancreatic islets were isolated from WF rats (275–300 g) by collagenase P (Roche Diagnostics, Italy) perfusion and purified by continuous-density Ficoll gradient as previously described (Longoni et al. 2010). Briefly, the pancreas was distended by bile duct injection of 15 mL of 4 °C-cold collagenase P (1 mg mL^{-1}; Roche Diagnostics) diluted in HEPES-buffered HBSS (Sigma-Aldrich), and then excised and minced. PIs were digested at 37 °C for 20 min under constant stirring. Islets were separated from exocrine tissue by centrifugation on a Histopaque (Sigma-Aldrich) discontinuous gradient, removed from the interface of the layers, washed in HBSS and finally resuspended in 10 mL of RPMI (Eurobio) supplemented with 10% fetal calf serum (Eurobio), 1% L-glutamine, 10 mM glucose (Sigma-Aldrich), penicillin (50 U mL^{-1}, Eurobio), streptomycin (50 μg mL^{-1}; Eurobio), amphotericin B (0.2 μg mL^{-1}; Eurobio) and 1% HEPES buffer (Sigma-Aldrich) in a free-floating culture flask. PIs were handpicked under an inverted microscope under sterile conditions and purity was assessed by dithizone staining (Sigma-Aldrich).

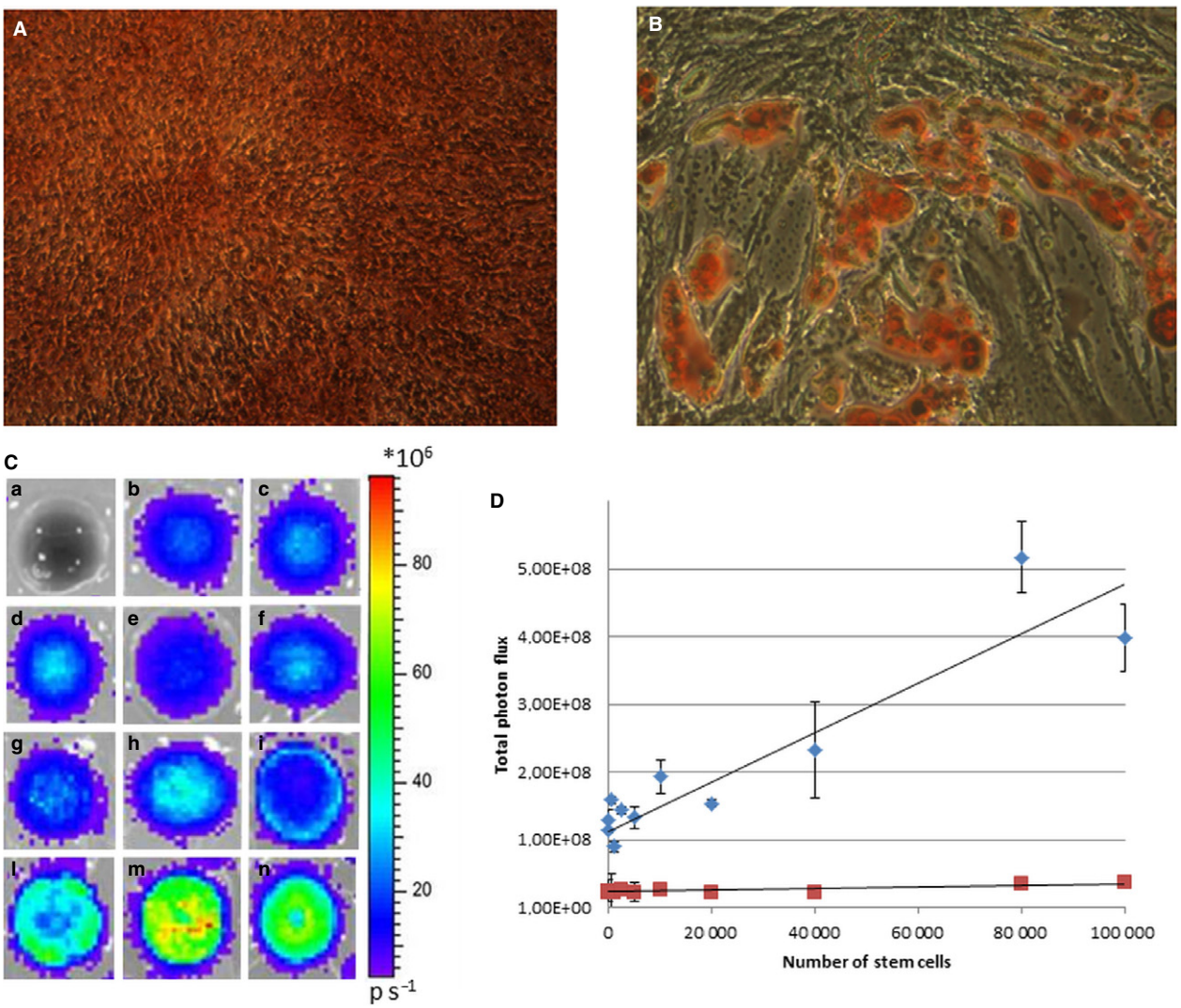

Fig. 1 Differentiation of MSCs. (A) Osteocytes, with visible deposits of hydroxyapatite stained intensely red with of Alizarin S, (B) orange–red-stained lipid vacuoles of the cytoplasm of MSCs treated with adipogenic medium with Oil Red-O. (C) Fluorescence images of nonfluorescent wells containing varying amounts of MSCs labeled with Qdots 800: a) control – no cells, b) 50 cells, c) 100 cells, d) 500 cells, e) 1000 cells, f) 2.5 × 10^3 cells, g) 5 × 10^3 cells, h) 10 × 10^3 cells, i) 20 × 10^3 cells, j) 40 × 10^3 cells, k) 80 × 10^3 cells, l) 100 × 10^3 cells. (D) Signal intensity of fluorescence images of nonfluorescent wells containing varying amounts of Qdots-labeled (blue squares) or unlabeled (red squares) cells. Acquisition modality: fluorescence with filters ex/em = Cy5.5 (615–665 nm)/ICG (810–875 nm).

For each graft, the total islet mass was expressed as the 150-μm-diameter islet equivalent number, calculated on the basis of volumetric assumptions. PIs were incubated at 37 °C (95% air and 5% CO_2), for 1–2 days before transplantation. The amount of PIs needed to transplant in $n = 2$ recipients was labelled with SPIOs (Endorem®, Guerbet, France) according to previously published methods (Marzola et al. 2009; Longoni et al. 2010).

Transplantation of PIs and MSCs

The effect of MSC intravenous administration was assessed in an allogeneic graft using Wistar Furth rats as donors and Lewis rats as recipients of PIs. Lewis rats were divided into four groups. Group 1 ($n = 6$) received saline intravenously (i.v.). Group 2 ($n = 6$) received 5×10^5 unlabelled MSCs i.v. Group 3 received 5×10^5 MSCs labelled with Qdots i.v. ($n = 12$; $n = 6$ rats were sacrificed 5 days and $n = 6$ rats 10 days after i.v. injection). Group 4 was divided in two subgroups: in the first one (4a) the rats received 700 IE islets in a portal vein and 5×10^5 MSCs labelled with Qdots i.v. ($n = 12$; $n = 6$ were sacrificed 5 days and $n = 6$ rats 10 days after i.v. injection). Animals belonging to the other subgroup (4b) ($n = 2$) received 700 IE islets labelled with SPIOs in a portal vein and 5×10^5 MSCs labelled with Qdots i.v., and were sacrificed 10 days after transplantation of PIs and i.v. injection of MSCs.

Lewis rats (230–250 g) were anaesthetized (Zoletil 100: tiletamine 90 mg kg^{-1} and zolazepam 10 mg kg^{-1}, Virbac s.r.l., by intraperitoneal injection) and the portal vein was exposed through a midline incision parallel to the spine. PIs suspended in 200 μL of PBS solution were injected and re-flushed two to three times into the portal vein. An amount of 5×10^5 MSCs labelled with QDots (or the same amount of unlabelled MSCs) were transplanted in L rats by i.v. injection in the tail vein. After 5 or 10 days, the animals were sacrificed and perfused with PBS. The following organs were excised: liver, lungs, spleen, kidneys and pancreas.

Imaging *in vivo* and *ex vivo* experiments

The rats of the subgroup 4b were anaesthetized (0.5–1% isofluorane) and placed into a 7.2-cm i.d. transmitter-receiver birdcage coil. MRI *in vivo* acquisitions were performed 10 days after transplantation using a 4.7 T 33-cm bore horizontal magnet (Oxford Ltd., Oxford, UK). Acquisition protocol was described in Marzola et al. (2009).

Fluorescence images were acquired using a VivoVision Systems, IVIS® 200 Series, for small laboratory animals (Caliper, Alameda, CA, USA). The system is made of a camera sensor back-thinned, back-illuminated, grade CCD 1 (2.7 × 2.7 cm, −90 °C), with a minimal image pixel resolution of 20 μm (pixel dimension 13.5 μm, imaging pixels 2048 × 2048), quantum efficiency > 85% between 500 and 700 nm, and > 30% between 400 and 900 nm. For the experiments we used a fluorescent modality with Cy5.5 (615–665 nm) excitation filter and ICG (810–875 nm) emission filter. Images were acquired with binning factor = 8, field of view = 12.8 cm, exposure time = 1 s, opening of diaphragm (f/stop) = 2.

Ex vivo fluorescence images of excised organs from all the experimental groups were acquired and analysed using Living Image 4.1 software (Caliper). According to Yukawa et al. (2012) the quantification of fluorescence emission of different excised organs was performed by considering the parameter RFI (ratio of fluorescence intensity), defined as follows: RFI = (fluorescence intensity of the organ)/(total fluorescence intensity of the five excised organs of the same animal: liver, kidneys, lungs, spleen, pancreas). Data analysis and statistics were carried out using routines written in MATLAB 7.1 (The MathWorks Inc., USA). A *t*-test analysis was performed with a significance level of $P \leq 0.05$.

Results

Characterization of MSCs *in vitro*

Rat bone marrow-derived MSCs were purified by plastic adherence. After the fifth passage, the cells grew exponentially, requiring weekly passages. MSCs treated with osteogenic medium formed small deposits of hydroxyapatite intensely red stained with Alizarin S (Fig. 1A). Treatment with adipogenic medium differentiated MSCs towards adipogenic lineages with Oil Red-O staining (Fig. 1B). Cytofluorimetric analysis showed the existence of a homogeneous population of adherent cells (after four to five passages), positive for CD90, CD44, CD54, CD73 and CD106. There was no significant contamination of haematopoietic cells, as flow cytometry was negative for markers of haematopoietic lineage, including CD11b and CD45 (data not shown).

The MSC labelling was observed *in vitro* by OI in fluorescence modality in order to assess the sensitivity of the technique. Images of wells containing different amounts of labelled or unlabelled cells are shown in Fig. 1C. The dependence of fluorescence signal intensity on the cell number is shown in Fig. 1D for labelled and unlabelled cells. A good correlation was found between signal intensity of wells containing labelled cells and the number of cells itself ($r^2 = 0.84$).

A slight decrease of the total flux at the highest number of cells was observed, probably due to the optical thickness of the cells. The fluorescence signal acquired in non-fluorescent wells containing pure DMEM or unlabelled cells was significantly lower than the signal acquired in wells containing labelled cells (Fig. 1). Even at the lowest number of cells investigated ($n = 50$), the fluorescence signal ($1.14 \pm 0.03 \times 10^8$ photon s^{-1}) was substantially higher compared with pure DMEM ($2.47 \pm 0.33 \times 10^7$ photon s^{-1}) or to 50 unlabelled cells ($2.20 \pm 0.42 \times 10^7$ photon s^{-1}). This result indicates an *in vitro* detection limit of about 50 cells.

Imaging *in vivo* and *ex vivo* experiments

The rats of subgroup 4b were imaged by MRI to monitor the presence of PIs labelled with SPIOs into the liver (Marzola et al. 2009; Longoni et al. 2010). Figure 2 shows a representative *in vivo* MR image of rat transplanted with PIs labelled with SPIOs 10 days after the PI transplantation. *In vivo* MRI acquisitions showed the image of the animal with PIs unlabelled (Fig. 2A) with respect to the image of hepatic parenchyma, with several dark spots corresponding to labelled PIs (Fig. 2B), confirming data described in Marzola

et al. (2009). No differences were found in the fluorescent light signal coming from the explanted liver between the animal of subgroup 4b and the animal of subgroup 4a, suggesting that no significative absorption of fluorescent emission can be attributed to the opacity of the MRI contrast agent.

The presence of labelled MSCs in different organs was studied *ex vivo* by fluorescence imaging.

Figure 3 shows fluorescence images of excised organs of representative rats sacrificed 5 (Fig. 3A) and 10 (Fig. 3B) days after injection with unlabelled MSCs (group 2), labelled MSCs (group 3), labelled MSCs plus transplantation of PIs (group 4). Qualitatively, the fluorescence signal emitted from organs of animals belonging to group 4 (MSCs and PIs) is higher than in the other experimental groups, suggesting longer duration of MSCs in the body. Organs excised from animals belonging to group 1 (saline) had a fluorescence emission comparable to organs excised from animals belonging to group 2 (images not shown). Data were then quantitatively analysed. To assess the possible effect of co-transplantation of PIs on MSC homing; data from animals belonging to experimental groups 3 and 4 (labelled MSCs) were compared by considering the RFI index previously defined (see Fig. 3C). Five days after transplantation, the fluorescence emission in liver of animals belonging to group 4 was significantly higher than in group 3, indicating that transplantation of PIs promotes homing of MSCs in the liver. The organs of group 4 were representative of all organs of subgroups 4a and 4b. The difference is not statistically significant in other organs (except lungs). For example, although the kidney fluorescence in group 4 is qualitatively much higher than in group 3, the difference is not statistically significant when data are analysed using the RFI index.

Discussion

In recent years, research in cell therapy for regenerative medicine has considered MSCs with increasing interest. MSCs have been largely applied in tissue regeneration models, in transplantation and for the treatment of several degenerative pathologies. Data derived from these studies have shown that MSCs may be a safe and realistic therapy for clinical use. Strictly related to the above-mentioned applications of MSCs is the need to monitor the fate of transplanted cells, and indeed several recently published papers have investigated their homing and biodistribution in animal models. Moreover, as many applications of MSCs have been performed in association with other cell types, it is very important to develop bimodal imaging methods to make it possible to follow the fate of different kinds of transplanted cells. Fluorescent Qdots were used here to label stem cells and they are widely used in preclinical studies, but their chemical composition, in particular the presence of cadmium in their core, prevents clinical application. For clinical use, nanoparticles with different chemical composition could be used in the future, but the optical thickness of the human tissue could represent a very important issue for fluorescence imaging.

In the present work, we investigated the homing of MSCs in an animal model of PI transplantation by bimodal imaging techniques. MSCs were labelled using fluorescent probes, whereas PIs were labelled with magnetic nanoparticles. Optical and MR imaging allowed detection of cells homing in different organs. When only MSCs are transplanted, the fluorescence signal emitted by excised organs, 5 or 10 days after injection of labelled MSCs, is similar to the baseline level (i.e. approximatively equal to the fluorescence emitted in the animal receiving unlabelled MSCs; compare groups 2 and 3 in Fig. 3A,B). This finding indicates that MSCs are cleared from the body within these time intervals. In contrast, fluorescence emission in the liver in group 4, in which labelled MSCs were co-transplanted with PIs, was significantly higher than in group 3, in which only labelled MSCs were transplanted. No statistically significant difference was detected in other organs, except lungs. This result, together with the good linear correlation observed *in vitro* between the number of labelled MSCs and the fluorescence signal (see Fig. 1), demonstrates that MSCs, when co-transplanted with PIs, show preferential homing into the liver. Ten days after transplantation, such preferential homing is no longer detectable.

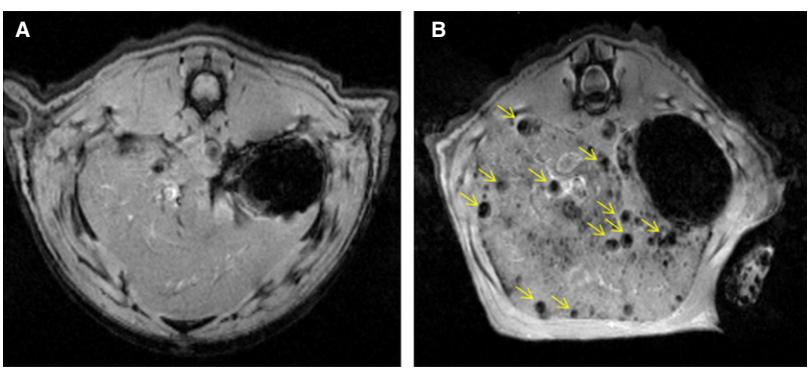

Fig. 2 MRI images of a representative animal with PIs unlabeled (A) and an animal with PIs labeled with superparamagnetic iron oxide particles (SPIOs) and MSCs labeled with Qdots (B).

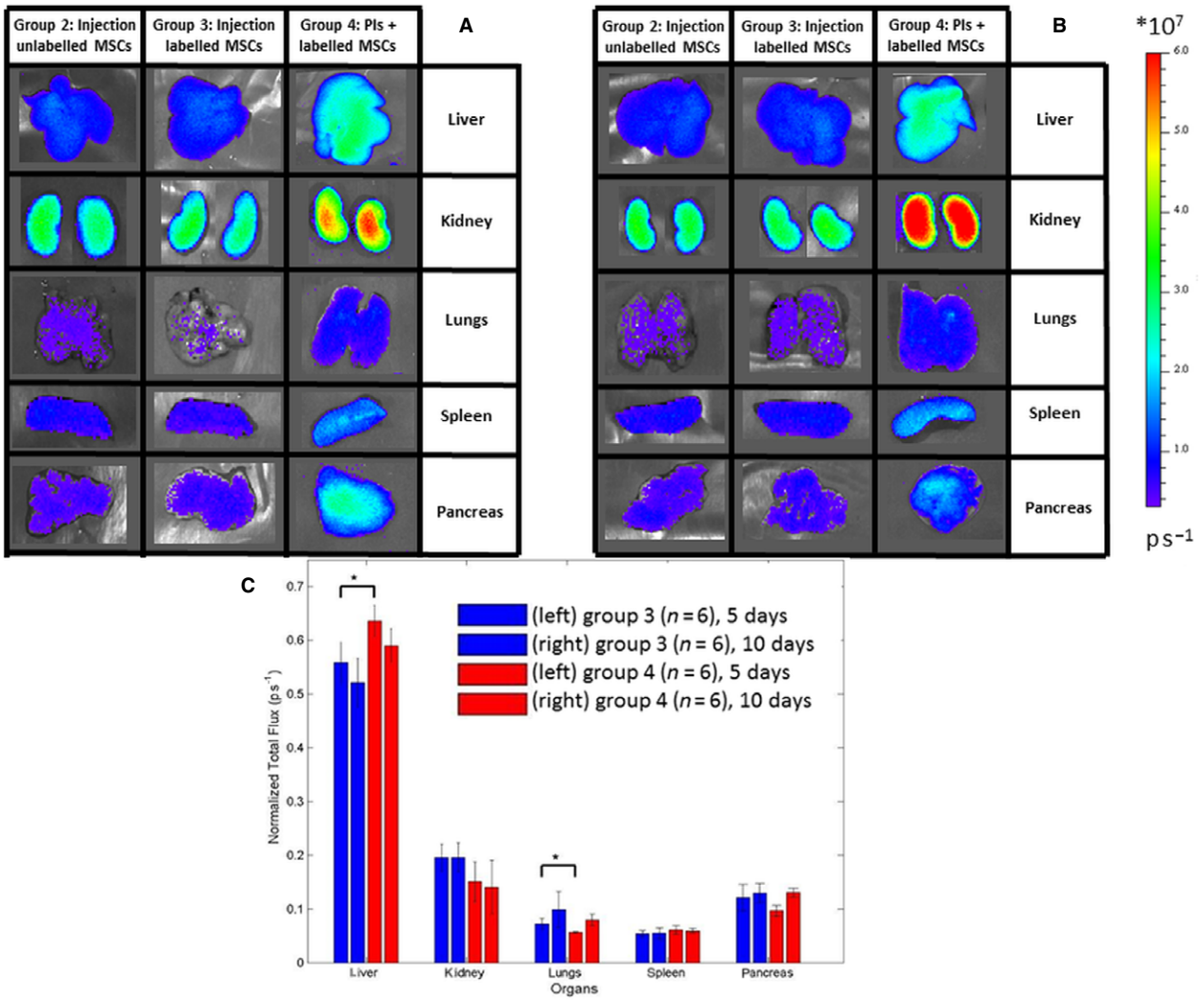

Fig. 3 Fluorescence images of excised organs of representative rats injected with MSCs and sacrificed 5 (A) and 10 (B) days after PIs transplantation. Group 2 rat injected i.v. with unlabeled MSCs; group 3 rat injected i.v. with labeled MSCs; group 4 rats injected i.v. with labeled MSCs and PIs. Acquisition modality: fluorescence with filters ex/em = Cy5.5 (615–665 nm)/ ICG (810–875 nm). Organs are shown here with different degrees of magnification. (C) Average signal emitted in different organs (RFI), $n = 6$ for each groups. Data are reported as mean ± SD over the different experimental groups. *T*-test analysis was performed, and statistical differences ($P \leq 0.05$) were indicated (*).

The high number of MSCs in liver observed when animals are transplanted with PIs may be correlated with inflammation and possible graft rejection of allogeneic islets. Indeed, it is well known that during an inflammation process (or tissue damage) MSCs are recruited by means of chemokines to the site of inflammation to suppress immune response and promote regeneration (Spaggiari & Moretta, 2013). The immunomodulatory effect of the MSCs is demonstrated in many *in vitro* studies showing that MSCs suppress T-cell proliferation, indicating immunosuppressive properties and reduced inflammation (Inoue et al. 2006; Le Blanc & Ringdén, 2007).

Several papers have examined the immunomodulatory effect of MSCs in the transplantation of PIs and in a previous study of this project, our group has also analysed (Longoni et al. 2010) the role of interferon gamma and granulocyte colony stimulating factor blood levels after PI and MSC inoculation; however, to the best of our knowledge the homing of MSCs has not been investigated in this model. Over the last 10 years, a number of studies have investigated *in vivo* the homing of SCs in a wide variety of other experimental diseases (Sohni & Verfaillie, 2013; Davey et al. 2014; Kavanagh et al. 2014; Ying et al. 2014). Most papers were based on MRI, but attention has recently been devoted to optical techniques in bioluminescence or fluorescence modality (Yukawa et al. 2012). Although many attempts have been made to reveal the MSC fate for surgical approaches within PI transplants, this topic needs to be analysed further. We transplanted PIs and injected MSCs in a single step in a single recipient and used a double

imaging approach to differentially monitor cellular homing. We used a bimodal acquisition system: fluorescence detection by OI to explore the homing of MSCs and MRI to investigate the fate of PIs. A limit of this approach is that OI suffers from relatively small penetration depth in living tissues that prevented us from working *in vivo*. This paper represents proof of concept that joint application of MRI and OI can allow simultaneous monitoring of the fate of transplanted cells.

Conclusions

We investigated the homing of MSCs labelled with QDots and i.v. injected in an animal model of PI transplantation (Marzola et al. 2009; Longoni et al. 2010). When unlabelled MSCs were injected, the fluorescence signal of the liver was not different from that of the controls (in which saline or unlabelled MSCs were injected). When MSCs were injected immediately after PI transplantation, the PIs were independently monitored with MRI and persisted in the liver for 10 days after the transplantation; the fluorescence signal of the liver was significantly stronger than in the control, showing that MSCs preferentially accumulate in the liver. This paper demonstrates that bimodal MRI and fluorescence imaging allows differential monitoring of the fate of two types of transplanted cells. Moreover, it shows that i.v. injected MSCs accumulate in liver when PIs have been transplanted in the same organ.

Acknowledgements

This work was supported by MIUR, projects PRIN 2005 and 2007, by Fondazione Cariverona (Verona, Italy) project 'Verona Nanomedicine Initiative' and by Fondazione ARPA. The authors would like to thank Prof. M. Malatesta (University of Verona, Italy) for revision of the manuscript.

References

Aly HA (2012) Cancer therapy and vaccination. *J Immunol Methods* **382**, 1–23.

Arifin DR, Bulte JW (2011) Imaging of pancreatic islet cells. *Diabetes Metab Res Rev* **27**, 761–766.

Blum B, Benvenisty N (2008) The tumorigenicity of human embryonic stem cells. *Adv Cancer Res* **100**, 133–158.

Bretzel RG, Hering BJ, Federlin KF (1995) Islet cell transplantation in diabetes mellitus – from bench to bedside. *Exp Clin Endocrinol Diabetes* **103**(Suppl 2), 143–159.

Davey GC, Patil SB, O'Loughlin A, et al. (2014) Mesenchymal stem cell-based treatment for microvascular and secondary complications of diabetes mellitus. *Front Endocrinol* **5**, 86.

De Feo D, Merlini A, Laterza C, et al. (2012) Neural stem cell transplantation in central nervous system disorders: from cell replacement to neuroprotection. *Curr Opin Neurol* **25**, 322.

Dobson KR, Reading L, Haberey M, et al. (1999) Centrifugal isolation of bone marrow from bone: an improved method for the recovery and quantification of bone marrow osteoprogenitor cells from rat tibiae and femurae. *Calcif Tissue Int* **65**, 411–413.

Domínguez-Bendala J, Lanzoni G, Inverardi L (2012) Concise review: mesenchymal stem cells for diabetes. *Stem Cells Transl Med* **1**, 59–63.

Evans MJ, Kaufman MH (1981) Establishment in culture of pluripotential cells from mouse embryos. *Nature* **292**, 154–156.

Gay RE, Resnick G, Kapoor N (1980) Characterization of human bone marrow fibroblast colony-forming cells (CFU-F) and their progeny. *Blood* **56**, 289–301.

Gurdon JB (2006) From nuclear transfer to nuclear reprogramming: the reversal of cell differentiation. *Annu Rev Cell Dev Biol* **22**, 1–22.

Hogan A, Pileggi A, Ricordi C (2008) Transplantation: current developments and future directions; the future of clinical islet transplantation as a cure for diabetes. *Front Biosci* **13**, 1192–1205.

Horwitz EM, Le Blanc K, Dominici M (2005) Clarification of the nomenclature for MSC: the international society for cellular therapy position statement. *Cytotherapy* **7**, 393–395.

Inoue S, Popp FC, Koehl GE (2006) Immunomodulatory effects of mesenchymal stem cells in a rat organ transplant model. *Transplantation* **81**, 1589–1595.

Kavanagh DP, Robinson J, Kalia N (2014) Mesenchymal stem cell priming: fine-tuning adhesion and function. *Stem Cell Rev* **10**, 587–599.

Le Blanc K, Ringdén O (2007) Immunomodulation by mesenchymal stem cells and clinical experience. *J Intern Med* **262**, 509–525.

Longoni B, Szilagyi E, Quaranta P, et al. (2010) Mesenchymal stem cells prevent acute rejection and prolong graft function in pancreatic islet transplantation. *Diabetes Technol Ther* **12**, 435–446.

Marzola P, Longoni B, Szilagyi E, et al. (2009) *In vivo* visualization of transplanted pancreatic islets by MRI: comparison between *in vivo*, histological and electron microscopy findings. *Contrast Media Mol Imaging* **4**, 135–142.

Nie H, Lee CH, Tan J, et al. (2012) Musculoskeletal tissue engineering by endogenous stem/progenitor cells. *Cell Tissue Res* **347**, 665–676.

Oishi K, Miyamoto Y, Murase K, et al. (2013) *In vivo* of transplanted islets labeled with a novel cationic nanoparticle. *PLoS One* **8**, e57046.

Patel SA, Sherman L, Munoz J (2008) Immunological properties of mesenchymal stem cells and clinical implications. *Arch Immunol Ther Exp (Warsz)* **56**, 1–8.

Przyborski SA (2005) Differentiation of human embryonic stem cells after transplantation in immune-deficient mice. *Stem Cells* **23**, 1242–1250.

Ricordi C, Strom TB (2004) Clinical islet transplantation: advances and immunological challenges. *Nat Rev Immunol* **4**, 259–268.

Sakata N, Chan NK, Chrisler J, et al. (2010) Bone marrow cell cotransplantation with islets improves their vascularization and function. *Transplantation* **89**, 686–693.

Sohni A, Verfaillie CM (2013) Mesenchymal stem cells migration homing and tracking. *Stem Cells Int* **2013**, article ID 130763, 8.

Spaggiari GM, Moretta L (2013) Cellular and molecular interactions of mesenchymal stem cells in innate immunity. *Immunol Cell Biol* **91**, 27–31.

Sutherland DE, Gores PF, Farney AC, et al. (1993) Evolution of kidney, pancreas, and islet transplantation for patients with diabetes at the University of Minnesota. *Am J Surg* **166**, 456–491.

Sykova E, Jendelova P (2007) *In vivo* tracking of stem cells in brain and spiral cord injury. *Prog Brain Res* **161**, 367–383.

Takahashi K, Yamanaka S (2006) Induction of pluripotent stem cells from mouse embryonic and adult fibroblast cultures by defined factors. *Cell* **126**, 663–676.

Ullah I, Subbarao RB, Rho GJ (2015) Human mesenchymal stem cells – current trends and future prospective. *Biosci Rep* **35**, pi: e00191.

Vittorio O, Quaranta P, Raffa V (2011) Magnetic carbon nanotubes: a new tool for shepherding mesenchymal stem cells by magnetic fields. *Nanomedicine (Lond)* **6**, 43–54.

Wei X, Yang X, Han ZP (2013) Mesenchymal stem cells: a new trend for cell therapy. *Acta Pharmacol Sin* **34**, 747–754.

Weimar B, Rauber K, Brendel MD, et al. (1999) Percutaneous trans hepatic catheterization of the portal vein: a combined CT- and fluoroscopy-guided technique. *Cardiovasc Intervent Radiol* **22**(4): 342–344.

Wu Z, Liu S, Hassink M, et al. (2013) Development and evaluation of ^{18}F-TTCO-Cys^{40}-Exendin-4 a PET probe for imaging transplanted islets. *J Nucl Med* **54**, 244–251.

Ying W, Xiaodong C, Wei C (2014) Plasticity of mesenchymal stem cells in immunomodulation: pathological and therapeutic implications. *Nat Immunol* **15**, 1009–1016.

Yoon SW, Kim DK, Kim KP (2014) Rad51 regulates cell cycle progression by preserving G2/M transition in mouse embryonic stem cells. *Stem Cells Dev* **23**, 2700–2711.

Yukawa H, Watanabe M, Kaji N (2012) Monitoring transplanted adipose tissue-derived stem cells combined with heparin in the liver by fluorescence imaging using quantum dots. *Biomaterials* **33**, 2177–2186.